The Quantum Computer: The Next Wave

Rajdip Ghosh, Bhushan Nadkarni, Eric Laird, Tak Au

12/14/05

EL553/PH549

Professor Wolf

The Quantum Computer: The Next Wave

For certain tasks, traditional computers have proven to be insufficient. In want of greater processing power to solve these tasks, various alternative computing schemes have been explored. With the fabrication of qubits becoming a reality, new solutions to old problems have been uncovered, even while the full extent of the power of the quantum computer has not yet been realized. This is due in part to the quantum Fourier transform, a transformation that allows a register of qubits to explore all possible outcomes to a given problem simultaneously.

Introduction

The emerging field of quantum computing offers immense possibilities in an exciting new branch of information science. For certain problems, the quantum computer can perform tasks that traditional computers cannot. Quantum computers make use of properties known as superposition and entanglement to process data. These properties allow speed benefits that tie up traditional computers indefinetly. To search a database of 10,000 items, a traditional computer requires a 5,000 step algorithm, whereas a quantum computer only requires 100. Perhaps the most dramatic example is in factoring numbers that are the product of two primes. Recently, a traditional supercomputing array at UC Berkley factored a 512-bit number in just under eight months. A single quantum computer with a sufficient number of qubits would be able to factor such a number in seconds. Software development is expanding the uses for quantum computing systems to previously impossible tasks. Libraries and programs are already available for the quantum computer in languages like LISP and PERL.

There have already been many hardware implementations of the quantum bit. So far, few have been scaled favorably up to usable computing levels. Here we will discuss one of the designs that has shown good scalability, the double quantum dot charge qubit. This design has also shown very precise readouts, solving yet another persistent proplem. A surge of interest in this design is helping to spur rapid developments.

In this paper we will show how qubits are prepared for computation and manipulated using the quantum fourier transform. Some simple vector mechanics of entanglement will be presented. Using this as our foundation, we will describe how Shor's algorithm is implemented. Next, a quantum logic circuit will be discussed. We will also describe some of the incarnations of the quantum computer. Lastly, Fabrication using “top-down” and “bottom-up” processes will be addressed.

Entanglement in a Qubit Register and the Quantum Fourier Transform

To explain how quantum information processing is done, we'll start with some definitions. An ordinary bit comprises one of two well-defined states, 0 or 1. So can a *qubit*, or quantum bit, but a qubit has a major advantage over an ordinary bit. A qubit in a state of *superposition* can have values of both "0" and "1" simultaneously. These two distinct cases can also be labeled ↓ and ↑. In superposition, the qubit will appear as a linear combination of these two states, $|\Psi\rangle = \alpha\,|\downarrow\rangle + \beta\,|\uparrow\rangle$ (see fig.1).

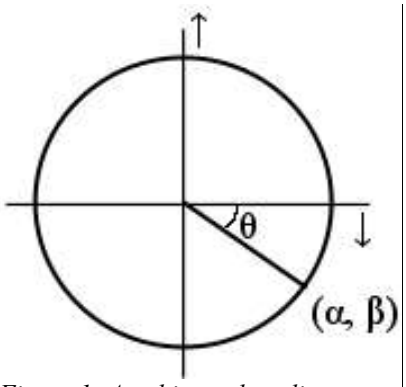

Figure 1: A qubit can be a linear combination of spin directions

$|\Psi\rangle$ is called the *wave function*, and it can be thought of as a position vector. The coefficients α and β can be any real numbers between -1 and 1, as long as $(\alpha + \beta)^2 = 1$.

Since a qubit can be a linear combination of states, a common illustration used to explain superposition is Schrödinger's cat. Erwin Schrödinger was a scientist who helped develop quantum mechanics, and Schrödinger's cat is a joke about a cat in a box with a poison capsule inside. The box is closed, and the capsule is timed to go off after a certain amount of radiation from a radioactive material triggers it. Because the material radiates particles at random intervals, the only way to know whether the cat is still alive is to open the box to see. The joke is that until the box is opened, the cat is in a state of superposition, wherein it is a linear combination of alive and dead until the measurement of opening the box occurs.

While the previous illustration is colorful, a cat in a box would not make a suitable qubit. A true qubit must satisfy a number of condititions, called the DiVicenzo criteria. First, a method for high fidelity readout is required. Second, the available spectrum of states must be perfectly distinct. Also, the time of superposition, or *coherence time*, must be long enough to allow error correction if needed. The number of qubits in the register has to scale, and requires a universal sets of gates. Finally, a 'reset' operation is required. In the example of Schrödinger's cat, the scalability and readout fidelity are both good, but the procedure clearly cannot be reset, and the distinguishibility of the two levels of the system is open to a certain degree of argument. It is also hard to imagine what error correction would entail.

A vital part of quantum information processing is *enganglement*. Consider a register of two qubits, $|\Psi\rangle_1$ and $|\Psi\rangle_2$. Entanglement occurs when these two qubits are in a state that cannot be subdivided into two qubits with simpler position vectors. Such a state would look something like this:

$$|\Psi\rangle = \alpha\,(\,|\downarrow\rangle_1\,|\downarrow\rangle_2\,) + \beta\,(\,|\uparrow\rangle_1\,|\uparrow\rangle_2\,) \qquad (\alpha+\beta)^2 = 1$$

Wheras an unentangled qubit pair might look like this:

$$|\Psi\rangle = \alpha^2(\,|\downarrow\rangle_1\,|\downarrow\rangle_2\,) + \alpha\,|\downarrow\rangle_1\,\beta\,|\uparrow\rangle_2 + \alpha\,|\downarrow\rangle_2\,\beta\,|\uparrow\rangle_1 + \beta^2(\,|\uparrow\rangle_1\,|\uparrow\rangle_2\,)$$

$$(\alpha^2 + 2\,\alpha\beta + \beta^2)^2 = 1$$

The subscript denotes which qubit the spin direction belongs to. Note that in the first example, the wave function is in its simplest form, and in the second example, the wave function could be broken down into two parts:

$$|\Psi\rangle_1 = \alpha\,|\downarrow\rangle_1 + \beta\,|\uparrow\rangle_1 \qquad |\Psi\rangle_2 = \alpha\,|\downarrow\rangle_2 + \beta\,|\uparrow\rangle_2$$

When the wave function can be divided like that, it means that the system is not entangled as it was in the former case. Such a system is called *biseperable*. A system may also be considered biseperable for higher orders of qubits if they can be broken into distinct entangled sets. A system of entangled qubits can not be factored into simpler parts, or for that matter, even distinguished as separate entities. To break the entanglement, the system must be disturbed or the coherence time must be allowed to lapse.

A special type of entanglement is called the *Bell state*. In the Bell state, the probability of finding either a ↓ or a ↑ is equal to ½. Mathematically, the Bell state looks like this:

$$|\,\Phi^{+}\rangle = \left(\frac{1}{\sqrt{2}}\right)(|\downarrow\rangle_1 \otimes |\downarrow\rangle_2 + |\uparrow\rangle_1 \otimes |\uparrow\rangle_2)$$

Another important type of entanglement is called 'Greenberger-Horne-Zeilinger entanglement', which is like Bell state entanglement only for higher orders. This type of entanglement is also called a 'W state' or even a 'Schrödinger cat state'. This is when 3 or more qubits are entangled so that at any time, only one of them is in a low-energy state $|S\rangle$, and the rest are in a higher energy, metastable state called $|D\rangle$ (calcium ions have a D-level lifetime $\tau \approx 1.16$s). An N-particle cat state looks like this:

$$|\,N \quad \mathrm{CAT}\rangle = \left(\frac{1}{\sqrt{N}}\right)(|\,D...DDS\rangle + |\,D...DSD\,\rangle + ... + |\,S...DDD\,\rangle)$$

This configuration is important for two reasons. For one, it is highly scalable, and so far, 8 qubits have been entangled in a cat state. Also, this kind of entanglement is very robust, even allowing particle loss under certain circumstances.

The next part is extremely complicated, but it is the backbone of quantum computing. Let's say we start with a register of *m* bits. The value of the register, *x*, will look like:

$$|\,x\rangle = |\,x_{N-1}\rangle\,|\,x_{N-2}\rangle ... |\,x_0\rangle$$

$$x = \sum_{m=0}^{N-1} x_m 2^m$$

Here x_m is the value of a particular bit in along the register. Together, these two formulae describe a binary number N digits long, with x_0 being the least significant bit, and x_{N-1} being the most significant bit. We now would like to define a set of variables, k_n, such that

$$k = \sum_{n=0}^{N-1} k_n 2^n$$

Crucially, we would like to pick n such that $n + m \geq N$. The values of k_n should be in reverse order compared with those in x_m. In experiment, $|k\rangle$ will be a register of qubits.

Now if we want, we can line up x's and k's in a table of bit representations.

x_{N-1}	x_{N-2}	...	x_{N-n-1}	...	x_1	x_0
k_0	k_1	...	k_n	...	k_{N-2}	k_{N-1}

Now we take a Fourier transform of this discrete set of data. A discrete Fourier transform will look something like:

$$A_N = \frac{1}{2^N} \sum_{j=0}^{N-1} f_j e^{\frac{2\pi i j p}{2^N}}, \quad p = 0,1,2,\ldots,N-1$$

This looks very much like our two previous series, but there is also a *phase factor*, $e^{2\pi ijp}$. Suppose we were to set $k = j$ and $x = p$. We now have a phase factor

$$e^{i 2\pi k x 2^{-N}} = \exp(i \, 2\pi \sum_{n=0}^{N-1} k_n \sum_{m=0}^{N-1} x_m 2^{n+m-N})$$

Which is true, since $\exp(i\, 2\, \pi\, 2^{n+m-N}) = 1$ if $(n + m - N) \geq 0$. We are now ready to take a Fourier transform of $|x\rangle$ by setting the highest digit of x equal to $r - 1$.

$$|x\rangle \rightarrow \frac{1}{2^{(r-1)/2}} \sum_{k_0 k_1 \ldots k_{r-1}=[0,1]} \exp(i \, 2\pi \sum_{n=0}^{r-1} k_n \sum_{m=0}^{N-r} x_{N-r-m} 2^{-(m+1)}) |k_0 k_1 \ldots k_{r-1} x_{N-1-r} \ldots x_1 x_0\rangle$$

Upon close examination, we can see that this transformation is actually two seperate transformations, which rotate some of the bits in the register. The first is for the 0^{th} qubit in $|k\rangle$ (or the r^{th} state in $|x\rangle$):

$$|0\rangle \rightarrow \frac{1}{\sqrt{2}}(|0\rangle + |1\rangle)$$
$$|1\rangle \rightarrow \frac{1}{\sqrt{2}}(|0\rangle - |1\rangle)$$

and the second is for the remaining states:

$$\exp(i \quad 2\pi k_r \sum_{m=1}^{N-r-1} x_{N-r-1-m} 2^{-(m+1)}) |k_0 \ldots k_r\rangle |x_{N-r-2} \ldots x_0\rangle = \ldots$$
$$|k_0 \ldots k_r\rangle \prod_{m=1}^{N-r-1} \exp(2\pi k_r x_{N-m-r-1} 2^{-(m+1)} |x_{N-m-r-1}\rangle)$$

And we're done! Collectively, these two transformations are called the *Quantum Fourier Transform* (QFT). They are used in every application of the quantum computer for which a regular computer is insufficient.

Qubit Rotation

Both of these transformations are called *rotations*. The first is a π/2 rotation, the second is a controlled *phase rotation* which transforms a single bit at a time. Recall that in figure 1, the circle has a position vector corresponding to the coefficients α and β. If we perform a phase rotation, it is often helpful to consider the phase angle, θ. Remembering Euler's formula,

$$e^{i\theta} = \cos\theta + i \quad \sin\theta$$

The implication here is obvious. We can model the phase factor of the resulting QFT as the angle θ. This is extremely convenient when considering large numbers of qubits.

In the case where qubits are calcium ions in a linear Paul trap (as is the case in a cat state- this will be explained in greater detail later) the rotation is performed on each ion individually using a "sideband" laser pulse of wavelength $\lambda \approx 728$nm. In this way, superposition can be engineered so that each qubit has predetermined values of α and β. The pulses are set so that the time for rotation π is determined, then the rotation can be performed. If we wish to organize qubits into a cat state, the phase shift is performed in a register of n qubits using the formula $\theta_n = \cos^{-1}(1/\sqrt{n})$ to find the angle of rotation.

Given a register of n qubits, each one has its own wave function. Since the qubit's wave function is discrete, we cannot say that it is continuous. However, we can say that each wave function (which we can picture here as a position vector) has a *distance*, δ, which is continuous. This "distance" is really a matrix of possible outcomes. A mathematical concept known as *Hilbert Space* is a way to generalize linear transformations such as the QFT. It can be shown that with entanglement of only a few dozen qubits, the corresponding Hilbert Space becomes enormous. This is what makes

the quantum computer useful for applications such as decryption or the traveling salesman problem, where the number possible outcomes quickly becomes very large. Although this is still a long way off, a quantum computer with 300 qubits has a potential outcome space greater than the number of protons in the universe.

An unfortunate consequence of performing computation with individual atoms or photons is demonstrated by the Heisenberg uncertainty principle:

$$\Delta x \Delta p_x \geq \frac{\hbar}{2}$$

Here, p_x and x are the momentum of the particle and its position, respectively. Should we wish to keep the particle's velocity small, it will be harder to know where the rotation should occur. The more we know about its location, the harder it will be to keep still.

Since our our ability to address an individual particle is limited by the uncertainty principle and various technological shortcomings, there are also limits to how good the *fidelity* is. Fidelity is a measure of how well a system of qubits performs in comparison with anticipated results. In figure 2, we see the result of a fidelity measurement on a cat state. The measurement was compared with a Monte Carlo simulation, which basically means comparing random data from a probability density function with the result of the experiment. For instance, if we set an 8-qubit cat state to produce the results of rolls of an 8-sided die, we would expect each possible answer to emerge as the result about 1/8th of the time.

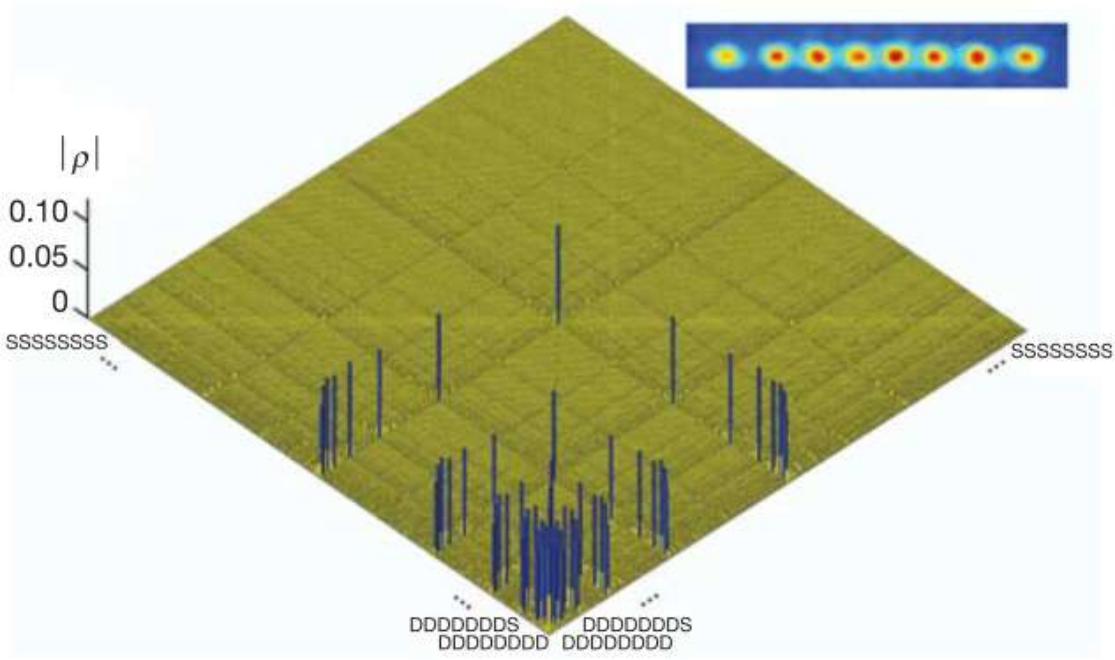

Figure 2: Fidelity matrix from an 8-qubit register. Ideally, blue lines should all have values of 0.125. Yellow lines indicate noise.

Recall the first transformation, where we rotated the k_0 qubit in the series. This transformation is known as the *Hadamard transform*, and when performed experimentally on a qubit, we say that the qubit has passed through a *Hadamard gate*. An imaginative depiction of a 4-qubit register is shown in figure 3.

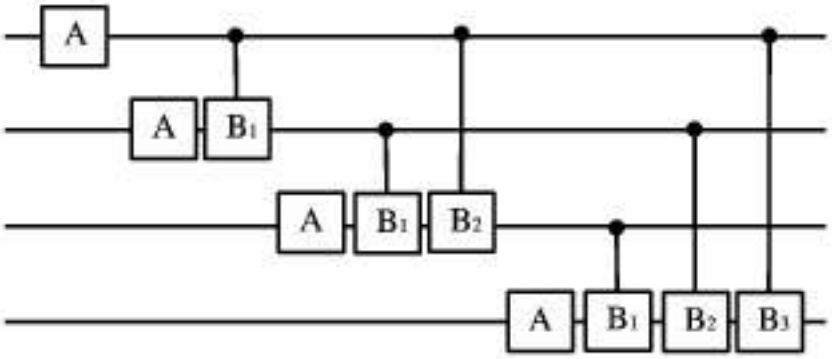

Figure 3: The quantum fourier transform applied to a 4-qubit register

In this figure, the Hadamard gate is gate A, and the gates B_i are phase operators. For any quantum algorithm, if the QFT is performed using this type of setup, there will be a high probability that the output will be the result that we are looking for. It should be noted that a qubit calculation will not result in the correct answer every time, because the result is probabilistic. However, the correct result of any quantum algorithm is typically found within 4-8 trials.

Shor's Algorithm

Shor's algorithm offers the way to factor a large number in a short of time using a quantum computer. This algorithm is fast under quantum computation because it is able to take advantage of the fact that a qubit can be in superposition. Shor's Algorithm is the result of an ingenious marriage of number theory, statistics, computer science and vector mechanics. The theory of how to factor numbers through Shor's algorithm is quite simple. Say we want to factor a number N; first, we introduce a number b which is between 0 and N. Raise the number b to the powers i = 1, 2, 3,…, and so on. We then find the mod (b^i,N) and let function F carry all the results. Once function F is large, we will find that function F is periodic and we can determine the period r of the function. Calculate the expression $A=b^{r/2}+1$ and $B=b^{r/2}-1$. Finally, the factors of N will be obtained by mod$[A,N]$ and mod$[B,N]$. A problem with this procedure is that it doesn't work for all functions F. Under classical computation, the function F must be recreated with a new starting number b. However, under quantum computation, all qubits are in superposition. In other words, all possible functions F are already computed. The only difficulty now lies in how to pick the right function F out of all the possible F. The following explanation shows how this algorithm works under quantum computation. First, there has to be $\log_2 N$ qubits in the input and the output register.

$$N^{-1/2} \sum_x |x\rangle \, |0\rangle$$

From the qubits, we generate the wave function, $f(x)$; that will give us:

$$N^{-1/2} \sum_x |x\rangle |f(x)\rangle$$

Then the system applies the QFT to the input register.

$$U_{QFT} |x\rangle = N^{-1/2} \sum_y e^{2\pi i x y / N} |y\rangle$$

This gives us the result…

$$N^{-1} \sum_x \sum_y e^{2\pi i x y / N} |y\rangle |f(x)\rangle$$

We may now divide the result from the output by N; and reduce the fraction to the lowest form. Let the denominator be r'. To check if the result is correct, we feed r' back into the equation $f(x+r') = f(x)$. Since $f(x)$ is a periodic function, the equation may be satisfied. However, if the result is wrong, we must pick a new y from the output register and perform the same test. If all outputs y don't satisfy the equation, this might mean that the coherence has collapsed at some point and the procedure must be restarted. A footnote to this procedure is that because a measurement is made directly, coherence will be destroyed. That is why the functions must go through a QFT in order for the probability of a favorable output to be high.

Paul Traps and Penning Traps

In order to implement such systems, there are many technological problems that will need to be overcome. All qubits must be trapped inside a confined area so that no disturbances will occur. One way to approach this is by using ion trap or a Paul trap. A Paul trap is based on the theory behind electric and magnetic fields. Figure 1 below show the schematic of Paul trap. Notice that the shape of the enclosure is hyperbolic. AC voltage is applied on both hyperbolic end electrodes and hyperbolic ring. The AC frequency is about 1 MHz.

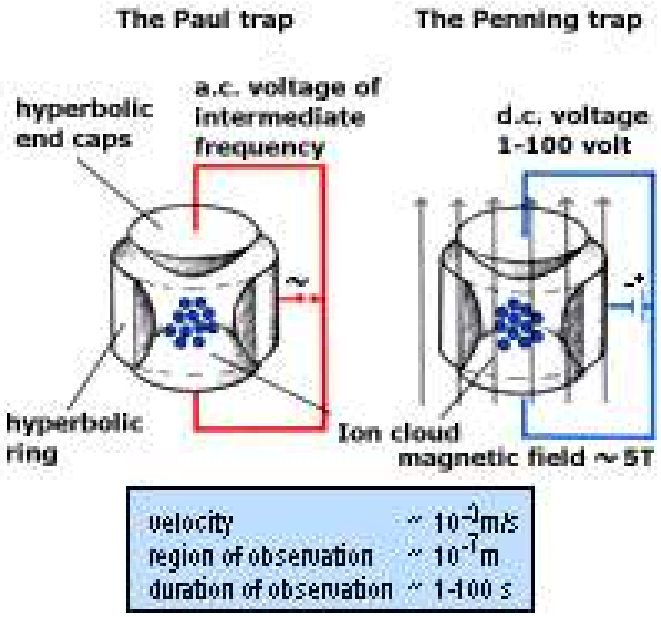

Figure 4: Paul trap (left) and Penning trap (right)

The motion of the particle is given by the equation:

$$\Phi\ (x,y,z,t\ ) = \frac{\Phi_0}{r_0^2}\left(\alpha x^2 + \beta y^2 + \gamma z^2\right)$$

And must satisfy the condition that

$$\Delta\Phi\ (x,y,z,t\ ) = 0$$

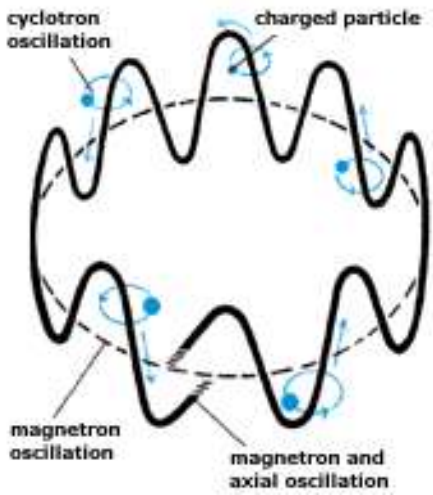

Figure 5: Oscillations of particles in a Paul trap

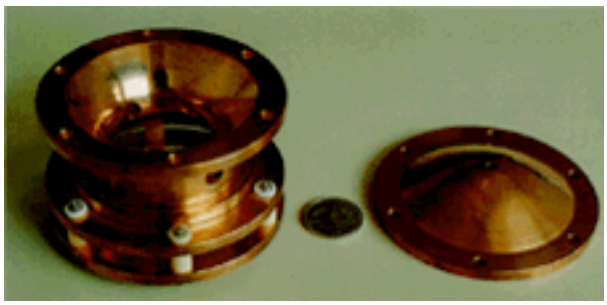
Figure 6: Paul trap

The way the AC voltage is applied, the trapped ions are first pulled up by the top metal electrodes and pushed in by the side electrodes. The ions are then pushed down by the bottom electrodes while being pulled outwards by the side electrodes. The process repeats. From this we get a motion that is represented in figure 2. This motion is described as a cloud in a small space. The Paul trap has another name known as Quadrupole trap because it has 4 magnetic poles. The actual trap is shown in the photo above (figure 6). The Penning trap is similar to the Paul trap except the ring electrodes are applied by DC voltage and there's a magnetic field (about 5T) applied outside of the trap.

By implementing traps, researchers can store ions in a confined region.

Coherence

In order for quantum computation to work, particles must be in *coherence*. That is, they have to remain in superposition for as long as possible. Accomplishing a workable coherence time isn't an easy task.

All the theories behind quantum computation are valid only as long as the

coherence of qubits holds. Therefore, it's important to look at some ways researchers try to keep the coherence to last as long as possible. Nuclear magnetic resonance, or NMR, allows the coherence of the qubit to last longer. The idea here is to use an atomic nucleus as the qubit. The surrounded electrons cloud is act as a shield from outside disturbances. So now, the qubit can "link up" in a molecule chain. Through this method, the superposition of the qubit can be held for about 1 second. NMR also allows the operator to change one particular qubit. However, the current problem is they can only link up to 7 qubits together. The problem with linking the qubit is that as more and more nuclei are tied together, the intensity of the qubit being measured will be decrease exponentially. This has the further detrement of lowering the fidelity of the readout. That's why it's difficult to perform any useful computation with such a system.

Another approach is to store data on photon. Photons don't interact with each other, but they do interact with electrons in an atom. If photon with right frequency is applied to excite an electron to move from the ground state up, the atom will radiate a photon when the electron falls back to the ground state. All that remains is to find a way to change the state of the photon in the process.

The CNOT Gate

Although quantum computation seems far out of reach, researchers have been making advances in the field. Researchers realized that all quantum operations can be implemented by single-qubit unitary and controlled NOT gates (CNOT). CNOT is defined as:

$$
\begin{aligned}
\oplus(|0\rangle_c\,|0\rangle_t) &= |0\rangle_c\,|0\rangle_t \\
\oplus(|0\rangle_c\,|1\rangle_t) &= |0\rangle_c\,|1\rangle_t \\
\oplus(|1\rangle_c\,|0\rangle_t) &= |1\rangle_c\,|1\rangle_t \\
\oplus(|1\rangle_c\,|1\rangle_t) &= |1\rangle_c\,|0\rangle_t
\end{aligned}
$$

A simple way to explain this is, if the controlling bit is zero, no changes will be made on the target bit; if the controlling bit is one, the target bit flips it state. One group used optical systems to demonstrate the functionally of CNOT to prove its concept. According to their paper "Demonstration of an all-optical quantum controlled-NOT gate, they produce all 4 bell states (show above) as a function of only the input logic values. The system that they assemble has the following schematics (figure 7):

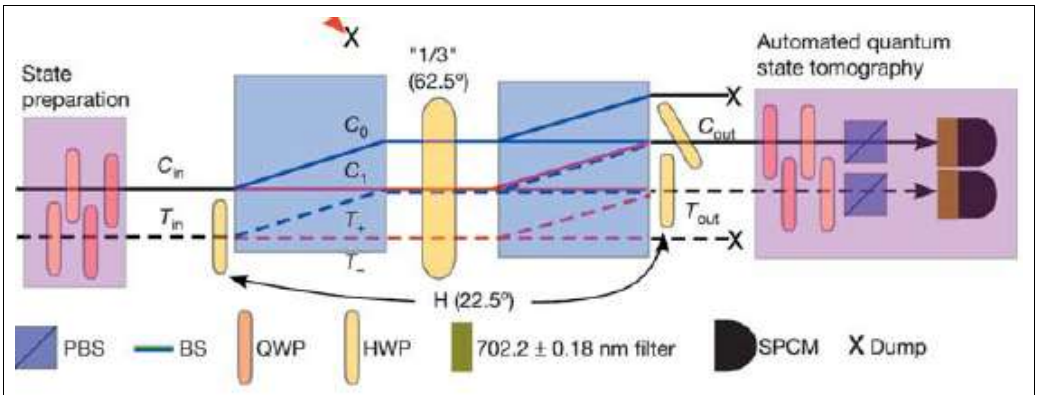

Figure 7: Schematic for an optical CNOT gate

They explained that this system works by having control and target qubits encoded by a single photon across two spatial modes. They prepare the states for both controlling and targeting qubit to have a form of any arbitrary superposition states:

$$\alpha\,|0\rangle + \beta\quad|1\rangle$$

Where the probability of the states is normalized by the function:

$$|\alpha|^2+|\beta\quad|^2=1$$

The targeting bits goes thru "1/3" beam splitter, where the states don't change (as long as there's no interference) by allowing C to state to be $|0\rangle$. However, if C is at state $|1\rangle$, they point out that interference will occur at the central "1/3" beam splitter. They claimed that there will be a π phase shift and the result will be:

$$\alpha\,|0\rangle + \beta\quad|1\rangle \rightarrow \alpha\,|1\rangle + \beta\quad|0\rangle$$

The controlling bit doesn't change from this operation. The way they tell the state is by its polarization. They express this as the following:

$$\alpha\,|H\ \rangle + \beta\quad|V\rangle \equiv \alpha\,|1\rangle + \beta\quad|0\rangle$$

After setting up the system, they test it by applying all possible inputs: $|C\rangle|T\rangle = |CT\rangle = |00\rangle, |01\rangle, |10\rangle$ and $|11\rangle$. Their results are shown in the fidelity graphs below:

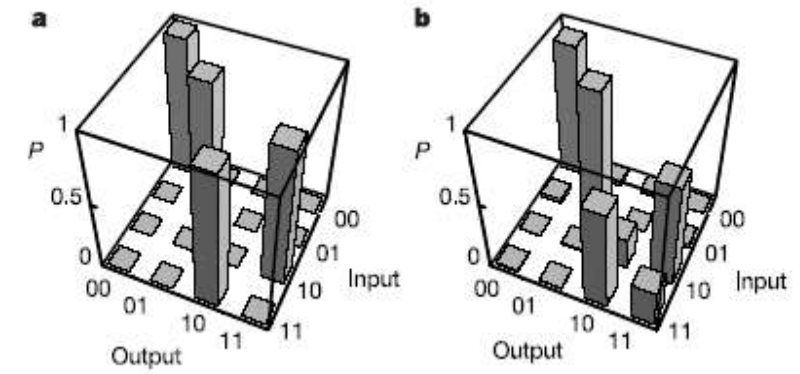

Figure 8: Fidelity of the optical CNOT gate

The left graph is the ideal case of what they would like to have as their result, the right graph is their actual result that they obtain using their designed system. They were able to make CNOT to work up to a point. However, when the controlling bit is at state $|1\rangle$, their result isn't as clear cut.

The Double Quantum Dot Charge Qubit

Here we discuss a fully-configured double quantum dot charge qubit based quantum computer device including on-chip detectors for registration of single ion implants, control gates accurately aligned to implanted donors and integrated single electron transistors (SETs) for qubit state read-out. Here we consider a Si:P dopant-based qubit in which the logical information is encoded on the charge degrees of freedom. This system, which is complementary to the Kane concept, is not dependent on single-spin readout.

The buried donor charge qubit is shown in Fig. 1 for the case of P dopants in Si, although a number of other dopant substrate systems could also be considered, such as GaAs:Si. The lowest two states of a single electron localized by the double well formed by two donor P+ ions give rise to a natural identification of the quantum logic states. External control over the barrier height and potential offset (or symmetry) is facilitated by B and S gates, respectively, placed above the buried P-P+ system, as in Fig. 1(b). With appropriate negative bias we can identify localized qubit states with high precision: $|0\rangle = |L\rangle$ and $|1\rangle = |R\rangle$, as shown in Fig. 1(c). Finally, a SET facilitates initialization and readout of the qubit.

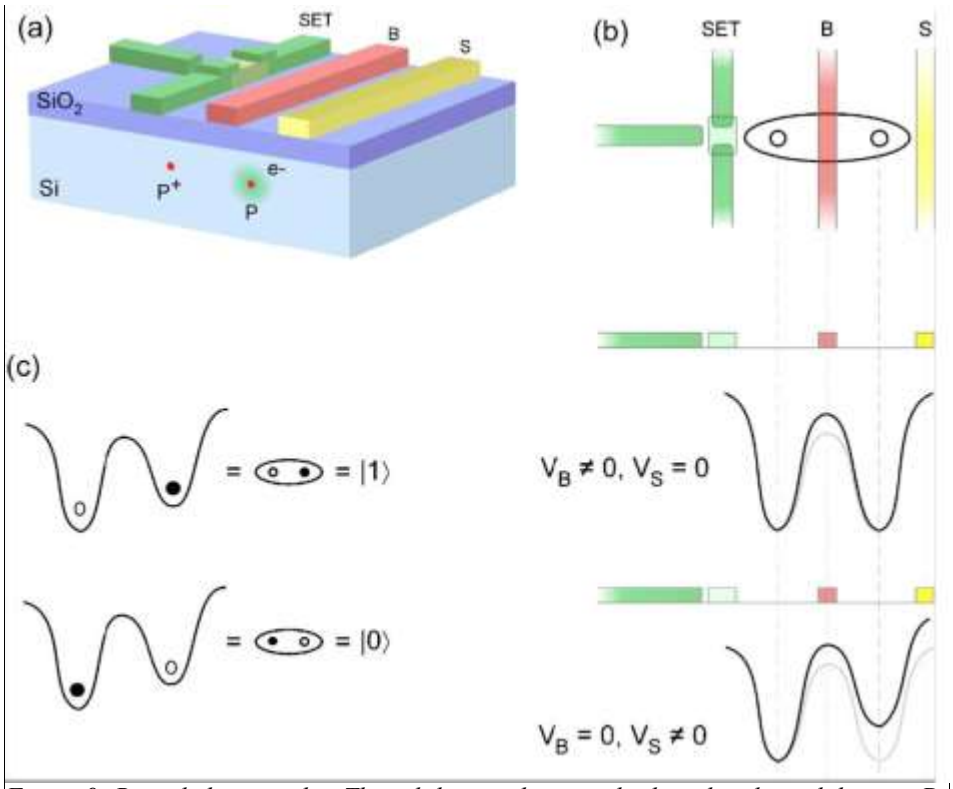

Figure 9: Buried charge qubit. The solid-state charge qubit based on buried dopants D, forming a D-D+ system with one electron, shown explicitly for the case for Si:P. The gated charge qubit showing barrier B gate and symmetry S gate control, together with a single electron transistor SET for charge based readout. One possible choice of logical states $|0\rangle$ and $|1\rangle$ defined is shown in terms of left- and right-localized states.

The key to understanding single-qubit gate operations is the effective Hamiltonian H_Q describing the dynamics of the P-P+ system in the presence of the S and B gates. In general, H_Q will be of the form $H_Q = h_0(t) + h_x(t)\sigma_x + h_z(t)\sigma_z$ where the σ_i operate in the basis of qubit states. The qubit logical states are defined by application of reference gate configuration voltages (V_B, V_S) and are manipulated by fast pulsed deviations ($\Delta V_B(t)$, $\Delta V_s(t)$) from the reference configuration. Under these conditions, the time-dependent coefficients can then be written as $h_i(t) = C_0^{(i)}(t) + C_s^{(i)}(t)\Delta V_S(t) + C_B^{(i)}\Delta V_B(t)$ with i=0,x,z. The qubit dynamics are thus determined by the parameters $C_B^{(i)}$, $C_B^{(i)}$, and $C_B^{(i)}$, which depend explicitly on the donor separation R and reference biases $\bar{V}_B$ and $\bar{V}_S$.

We have two choices for the basis of logical qubit states corresponding to the lowest two states being localized or delocalized. Since SET readout is most easily carried out for localized states, we choose initially the configuration with nonzero S-gate bias, which defines our qubit states as $|0\rangle = |L\rangle$ and $|1\rangle = |R\rangle$. Careful examination of the lowest two eigen states of HQ shows that for $\bar{V}_s \approx 0.1$ the qubit fidelity is optimal, with higher state amplitudes less than 10^{-4} in the logic states. After setting the reference gate configuration to $(\bar{V}_B, \bar{V}_S) = (0\,\mathrm{V}, 0.1\,\mathrm{V})$, the gate bias pulses ($\Delta V_B(t)$, $\Delta V_S(t)$) required for qubit control can be read off from HQ. For example, a $\pi/2$ rotation over 50 ps requires gate bias pulse values of ~(-0.40V, + 0.10V).

Immediately after fabrication the qubit must be preinitialized by removing one of the electrons from the P-P system to form the charge qubit. Using the S and B gates, the

electron in the right-hand donor well is ionized by a large S gate bias; at the same time, the B gate is raised to effectively isolate the electron in the left-hand well. After preinitialization, the SET conductance can be calibrated for the $|L\rangle$ and $|R\rangle$ states. Finally, initialization of the charge qubit into the left state $|0\rangle$ is effected by simply biasing the S gate and observing the SET conductance.

Prior to readout, the qubit is in a general state $|\psi\rangle = c_0|0\rangle + c_1|1\rangle$ resulting from a sequence of gate operations with the SET blockaded so that no current flows. To perform a projective measurement a voltage is applied to the SET gate, tuning it to a conductance peak—the current flow through the device decoheres the charge qubit strongly and causes a transition in time t meas,$T1$ to a statistical mixture of the localized eigenstates. Since the system has been calibrated in the preinitialization process, the SET will give a distinguishable reading $I_{L,R}$ corresponding to the system having collapsed into the left or right state with probabilities $|c_0|^2$ and $|c_1|^2$, respectively.

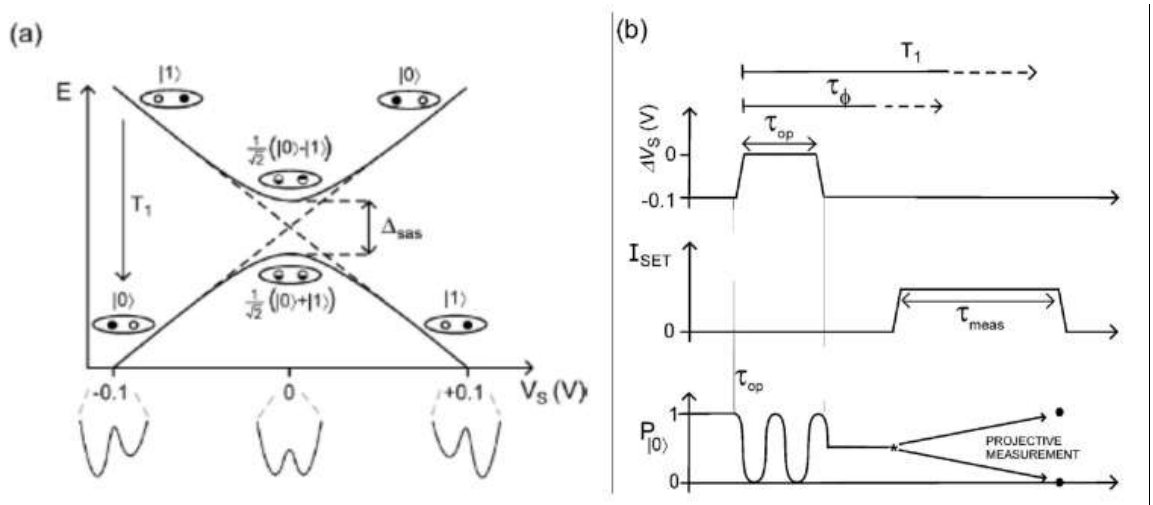

Figure 10: Qubit states and pulse timing. a) Energy diagram illustrating the evolution of the eigenstates of the system as a function of applied S-gate bias. b) Pulse timing diagram and SET readout showing the relative time scales for gate operation (top), SET readout (t means), dephasing (tf), and relaxation (T1).

Successful operation of quantum devices is contingent on coherence times remaining longer than the time required for arbitrary rotations. Primary sources of decoherence include phonons, Johnson noise on the gates, and materials-related charge noise. At mK temperatures the thermal phonon population is very small, but spontaneous phonon emission can still occur. A calculation of LA phonon decoherence for the P-P+ system at 100 mK concluded that for donor separations of 25 nm and greater, τ^{phonon} is of order μs. The corresponding phonon-induced error for a one-qubit NOT gate has recen been shown to be very low, while for s_x rotations an error of 3×10^3 was obtained. This error rate is, however, very sensitive to the phonon wavelength.

Many (100, 200 and 600) clusters implanted with either P or Si (control), few atom (5, 20) devices and two-atom devices implanted using single atom detection have been fabricated. Figures 3(a) and (b) show correlated SET data for 600-atom cluster devices. These data correspond to quasi-periodic charge transfer events detected by both surface SETs. The charge transfer loci can be seen to alter in angle with differing control gate sweeps. Figure 3(c) and (d) show equivalent data for control devices implanted with 600-atom Si clusters. These data show no clear transfer events suggesting that the

implantation and annealing process produces no large numbers of significant charge traps or defects.

The on-chip PIN detector structures are depicted in Figure 11. Figure 11(b) shows a scanning electron microscope image of the structure fabricated using optical lithography with carefully aligned p+ diffused regions, contact metal and a central thin oxide site for the finer device features. In Figure 11(c) a detection spectrum shows two 14 keV 31P+ ion impacts well above the noise threshold achieved with this structure. Data in Figures 11(d) and (e) show correlated SET data for devices implanted with nominally 5 atoms in total. There is a small number of transfer events observed as might be expected for such a device.

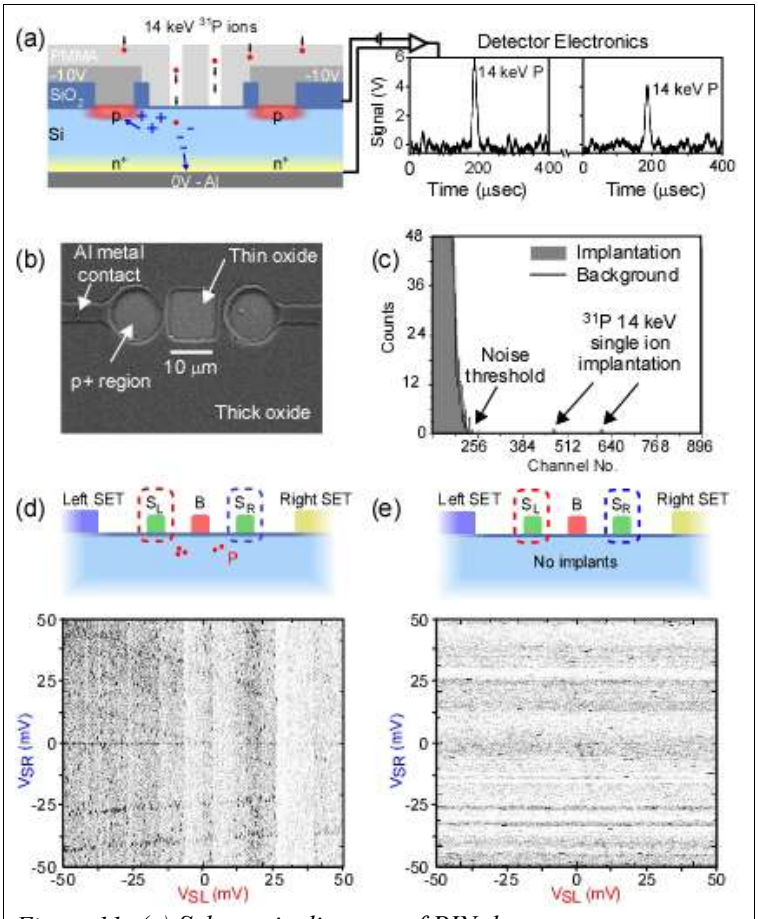

Figure 11: (a) Schematic diagram of PIN detector structures with real implant data for single 14 keV 31P+ ion impacts. (b) SEM image of PIN structure. (c) Detection spectrum showing two P atom strikes above the noise threshold. (d) and (e) Schematic and correlated SET data for few-P-atom and no atom (control) devices respectively

The Figure 12 shows Schematic of the correlated SET system for read-out of charge transfer of a double dot. The dots are connected via a tunnel junction and the charge configuration of the double dot is controlled with the gates labelled A1 and A2. SET 1 is more strongly coupled to the charge on dot 1 than the charge on dot 2, and SET 2 is similarly more sensitive to the charge on dot 2. (b) SEM image of the actual device

fabricated to realize correlated charge measurements. (c) Conductance traces showing the individual SET responses to charge motion (discontinuities in the conductance traces) on the double dot. (d) Upper panel: conductance traces where effects of the A gates on the SETs have been compensated for. Lower panel: correlation signals clearly showing the signature of charge transfer and rejecting noise due to background charge fluctuations. In parts (c) and (d) the solid lines denote SET 1 and the dotted lines denote SET 2.

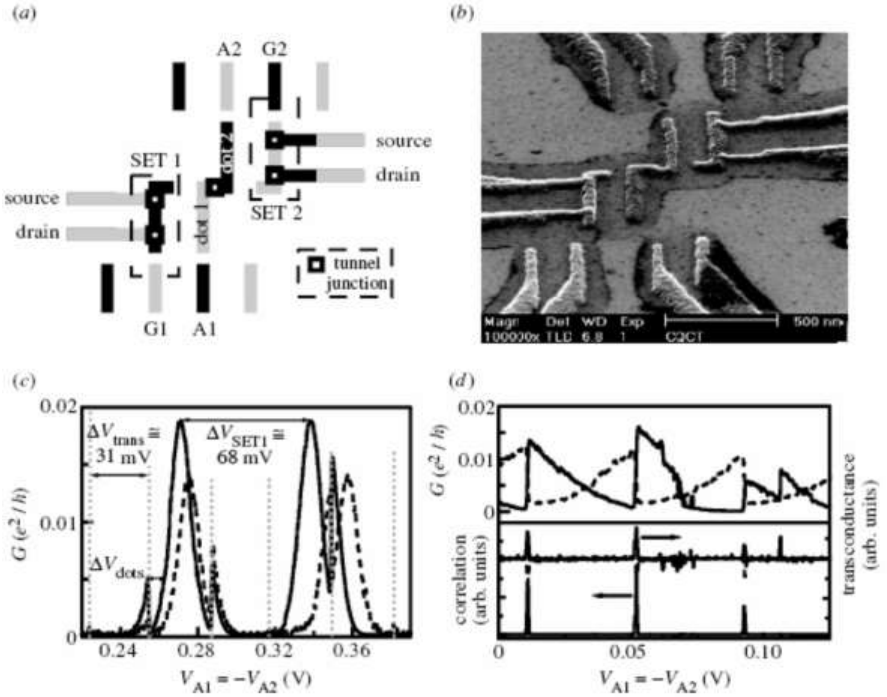

Figure 12 (a) Schematic of the SET system for readout of the double quantum dot. (b) SEM image of the device. (c) Conductance trace showing the responses to charge motion in the SET. (d) Conductance traces and correlation signal.

Bottom-Up Fabrication of Charge Qubit Devices

For qubit operation we require an atomically precise array of P nuclei embedded in silicon approximately 200 Angstroms apart, such that the donor electron wavefunctions can overlap, and an insulating barrier to isolate them from the surface control B- and S-gates. Using a combination of scanning tunnelling microscopy (STM) and molecular beam epitaxy (MBE) we employ a "bottom-up" strategy to build the device atomic layer by atomic layer. The final device structure, with the qubit architecture is shown in figure 13.

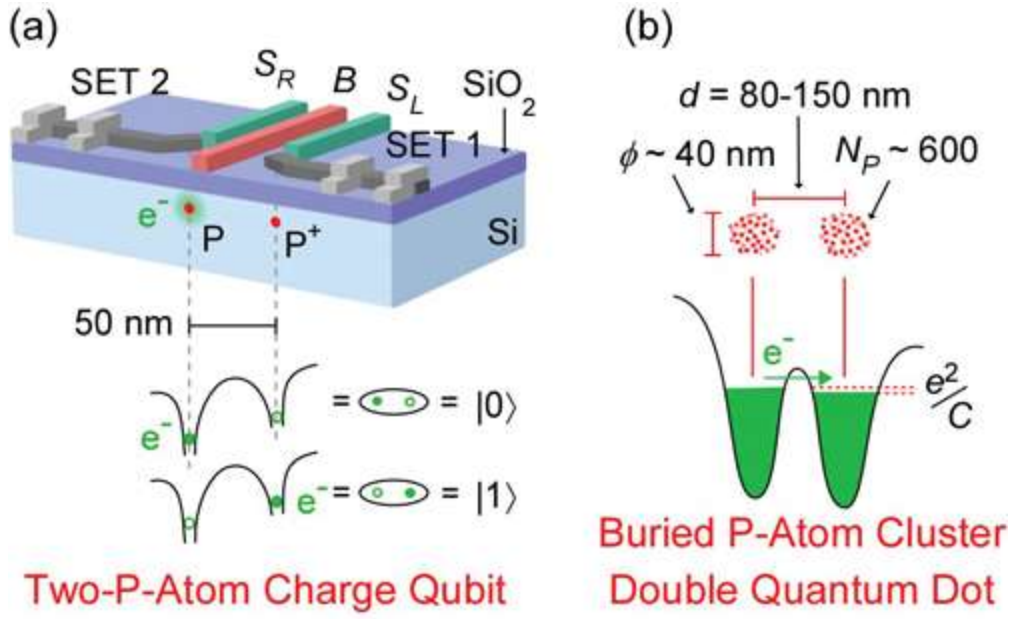

Figure 13: Device Structure

Figure 14 shows the detailed "bottom-up" fabrication strategy to build the quantum computer.

1. The clean, defect-free Si(001) surface is exposed to atomic hydrogen (H) which passivates the surface to form a monolayer (ML) of hydrogen resist.

2. The STM tip is then used to desorb single H atoms from the resist, thereby exposing the underlying Si substrate.

3. During subsequent exposure of the surface to phosphorus-containing molecules, such as phosphine (PH3) gas single PH3 molecules adsorb into the hole in the resist bonding directly to the silicon surface.

4. A critical annealing step incorporates the P atoms from the PH3 molecule into the Si surface while leaving the hydrogen resist layer unaffected. This step is important since it changes the weakly physisorbed phosphorus atom in the phosphine molecule with only one covalent bond to the surface into an incorporated phosphorus atom in the silicon surface with three covalent bonds. This helps to secure the phosphorus atom in its patterned location providing a stronger resistance to thermal diffusion in subsequent processing stages.

5. The hydrogen resist layer is removed from the surface without destroying the ordered array of phosphorus atoms.

6. The phosphorus atoms are then encapsulated in a few monolayers of silicon grown at room temperature to minimise dopant diffusion [4 ,5] out of the patterned arrays.

7. Subsequent rapid annealing reduces the defect density in the silicon layer and flattens the surface allowing us to image the dopants beneath the surface. A key factor in the silicon encapsulation process is to minimise heating of the sample as this may cause the phosphorus atoms to thermally diffuse or segregate to the surface, thereby destroying the carefully created STM patterned array.

8. Steps 8-10 The last three steps include Si growth at higher temperatures, the growth of an insulating barrier layer and registration of the P qubits to aligned surface metal gates.

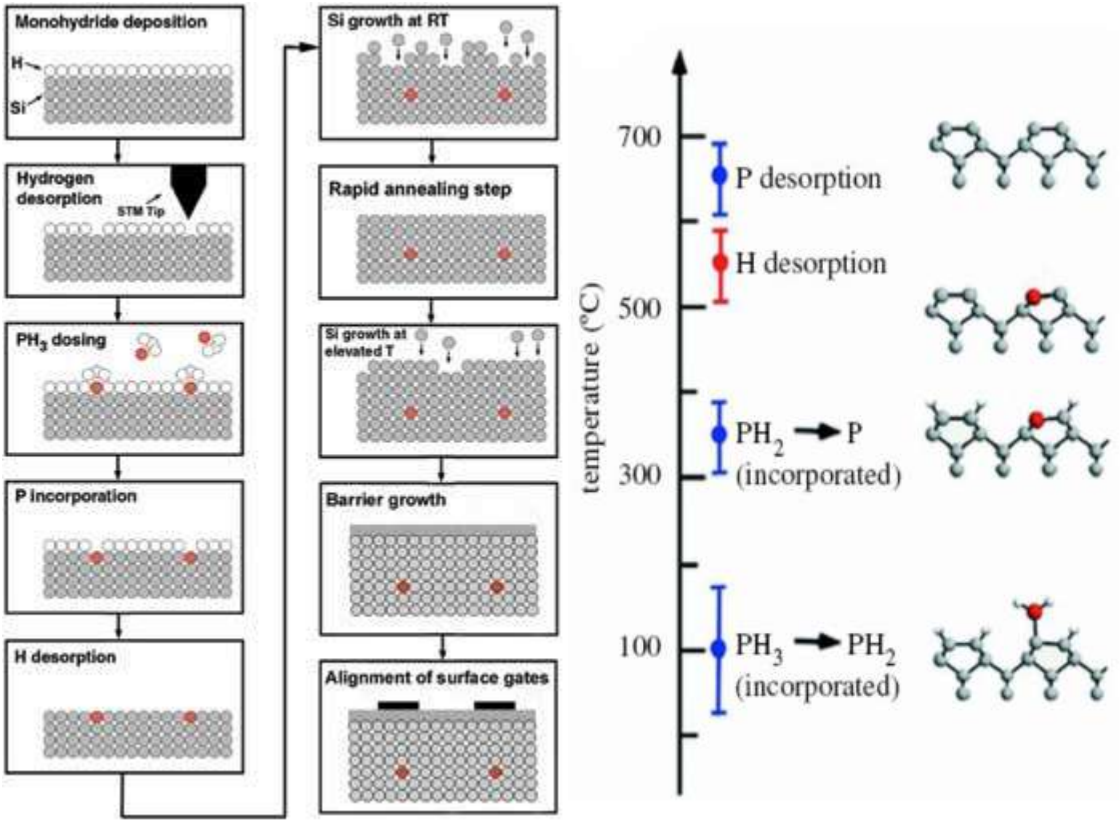

Figure 14: Bottom-up fabrication process

The fabrication of registered P qubit arrays has only become possible with the design of a combined customised STM-SEM/MBE system shown in figures 15 and 16. This system incorporates several unique features including the ability to image sample sizes of $1cm^2$, an SEM attached to the STM to allow precise tip positioning on the sample surface and observation of nanometer features on the surface, an optical position read-out to allow reproducible positioning of the STM tip several hundred nanometers from a registration marker on the surface (figure 15) and a full 4" SiGe capability for device quality silicon, sample uniformity and accurate growth rate calibration (figure 16).

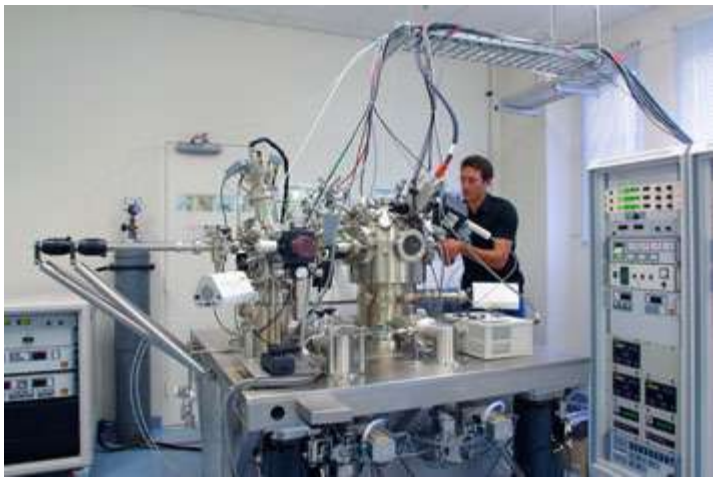

Figure 15Customized combined STM-SEM system

Figure 16: SiGe MBE system

After fabrication of the P qubit array it is then necessary to transfer the sample to the Semiconductor Nanofabrication Facility for subsequent B- and S-gate fabrication.

Top-Down Fabrication of Charge Qubit Devices

We now discuss the fabrication of a charge-based qubit scheme in silicon (see Figure 1). We develop a 'top-down' fabrication strategies for producing fully-configured quantum computer devices including on-chip detectors for registration of single ion implants, control gates accurately aligned to implanted donors and integrated single electron transistors (SETs) for qubit state read-out.

The `top-down' approach employs a low energy (keV) ion beam to implant the phosphorus atoms. Single-atom control during implantation is achieved by monitoring on-chip detector electrodes, integrated within the device structure.

Figure 17 depicts the technique developed to localize individual phosphorus atoms at the desired qubit array sites for a two-donor device. A nanopatterned ion-stopping resist such as poly(methyl methacrylate) (PMMA) denotes the array sites and a lowenergy (14 keV) $^{31}P^{+}$ ion beam is used to implant the P dopants to an average depth of 15 nm below the Si{SiO2 interface, for a 5 nm thick SiO2 layer.

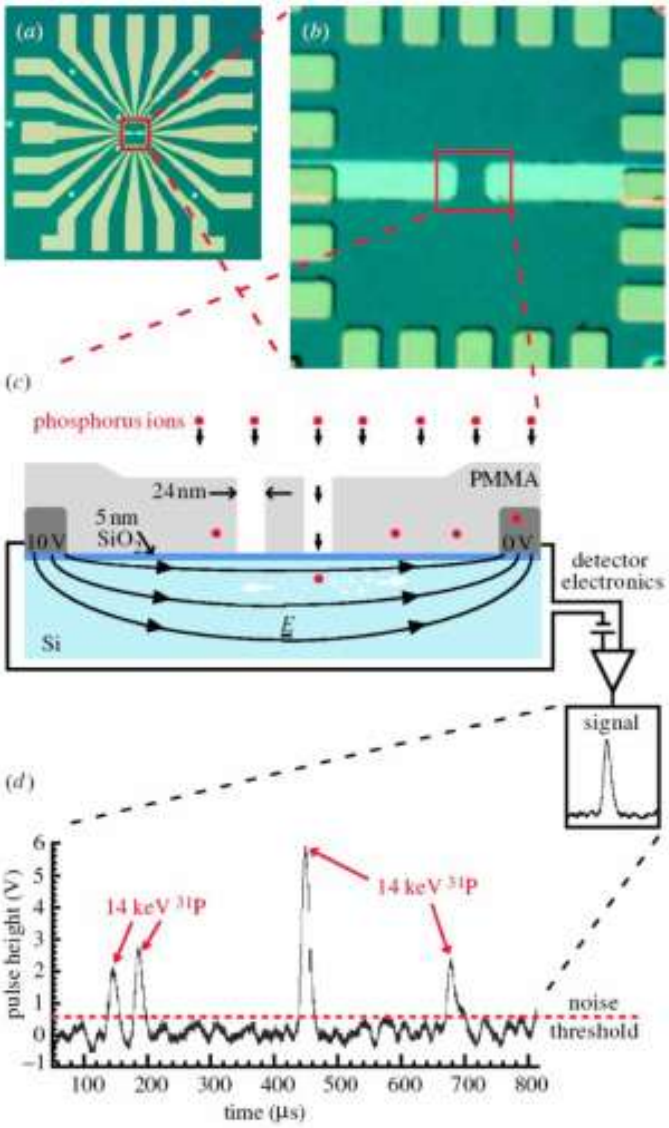

Figure 17: Electrically registered single-ion implantation. (a), (b) Optical images of detector electrodes.(c) Schematic showing phosphorus implantation through a resist mask. Each ion strike creates an electron/hole plasma, producing a current pulse monitored by on-chip electrodes.(d) Experimental demonstration of single-ion strikes in an i-Si substrate from a 14 keV phosphorus-ion beam.

The fabrication of a device such as that shown in figure involves a number of high resolution electron-beam lithography (EBL) steps, each of which must be aligned to

the others to within 20 nm. The process proceeds as follows:

1. A 5 nm thick SiO2 layer is thermally grown on a near-intrinsic silicon wafer, with a background n-doping level of 10^{12} cm^3.
2. If single-ion doping control is required, micrometer-scale aluminium detector electrodes are then deposited on the substrate using ultraviolet lithography.
3. To provide sub-20 nm alignment accuracy between all features on the device, Ti/Pt alignment markers are patterned using EBL.
4. In a second EBL step, two sub-30 nm apertures are opened in a layer of PMMA resist of thickness greater than 100 nm. The patterned PMMA resist acts as a mask for the phosphorus-ion implant step to follow.

The inset in figure 18 shows the result of a metallization and lift-off used to demonstrate the dimensions of these apertures. Following aperture definition, a 14 keV P+ ion beam is directed at the substrate to implant the donors. The PMMA layer is suffciently thick to stop the ions and forward recoil of H atoms from the PMMA itself, while ions which pass through the nano-apertures come to rest at a mean depth of 15 nm below the Si{SiO2 interface and register a current pulse in the on-chip detector circuit.

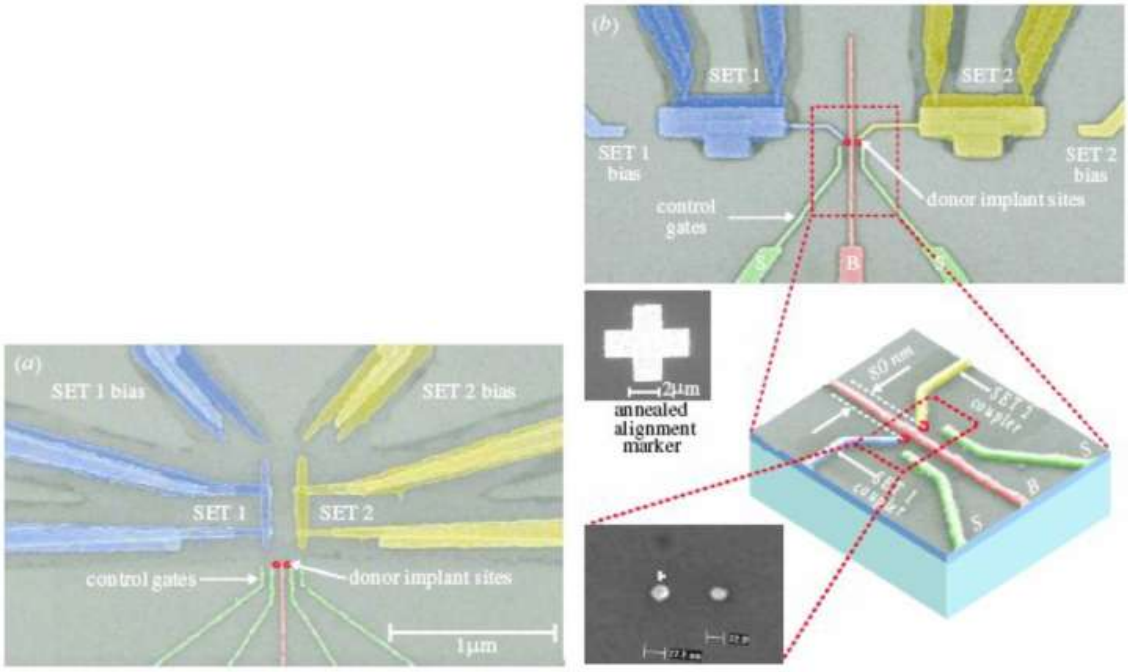

Figure 18: Scanning electron microscope (SEM) images of prototype devices incorporating buried phosphorus-ion implants. (a) Device with ¯ve control gates (bottom of image) to control electron motion between donors, together with two closely spaced SETs to detect electron transfer. (b) Modi¯ed device, where each SET island has a coupling electrode to capacitively couple it to a phosphorus donor site. A long central barrier (B) gate may be used to control tunnelling between donors. Inset, bottom left: demonstration of implantation apertures via metal lift-off .

5. Following calibrated implantation and resist removal, the samples are then subjected to a 950 C rapid thermal anneal (RTA) for 5 s to remove implant damage and activate the donors. The 5 s RTA process is necessary to limit P

donor diffusion to 1 nm.

6. Following ion implantation and activation, the remaining nanocircuitry on the surface of the chip is completed using two further EBL steps.
7. Firstly, the Ti/Au control gates are deposited following EBL patterning of a single PMMA layer. The gates on the devices in figure, produced using this process, all have line widths below 20.
8. Finally, the two Al/Al2O3 SETs are fabricated using a double-angle metallization process and a bilayer resist.

Preliminary electrical measurements on the device in figure indicates that the two SET islands were more strongly coupled to each other than to the phosphorus donors below them. A new architecture has recently been developed to decouple the two SETs, and is shown in figure. Here, the two SETs are separated by 1 mm. However, each SET island is connected to the central donor region using a Ti/Au coupling electrode. These are designed to capacitively couple each SET to its target donor atom or atom cluster, but not to its neighbouring SET. To provide further isolation, a long barrier (B) gate is configured between the two donor clusters and SET couplers.

1. http://en.wikipedia.org/wiki/Shor's_algorithm

2. http://nobelprize.org/physics/laureates/1989/illpres/trap.html

3. http://en.wikipedia.org/wiki/Paul_trap

4. http://beige.ucs.indiana.edu/M743-talk-2/node8.html

5. http://www.physics.uq.edu.au/people/andrew/publications/2003/cnot.pdf

6. David P. DiVincenzo, "Double Quantum Dot as a Quantum Bit", Vol 309-Science, Sep 2005.

7. Xuedong Hu, Belita Koiller, S. Das Sarma, "Charge qubits in semiconductor quantum computer architectures: Tunnel coupling and decoherence", 13 Dec 2004.

8. L. C. L. Hollenberg, A. S. Dzurak, C. Wellard, A. R. Hamilton, D. J. Reilly, G. J. Milburn, and R. G. Clark, "Charge-based quantum computing using single donors in semiconductors", Physical Review B 69, 113301 (2004).

9. R. G. Clark, R. Brenner, T. M. Buehler, V. Chan, "Progress in silicon-based quantum computing", The Royal Society, 11 June 2003.

10. Centre for Quantum Computer Technology, Australia, http://www.qcaustralia.org/crp_asd.htm

11. K. Bladh, D. Gunnarsson, G. Johansson, A. K¨ack, G. Wendin, P. Delsing, "Reading out Charge Qubits with a Radio Frequency Single Electron Transistor", PACS numbers: 03.67.Lx, 73.23.Hk, 85.25.Na, April 19, 2002.